Available online at www.sciencedirect.com
ScienceDirect
C. R. Physique 9 (2008) 418–426
COMPTES RENDUS PHYSIQUE
http://france.elsevier.com/direct/COMREN/

Materials subjected to fast neutron irradiation/Matériaux soumis à irradiation par neutrons rapides

Atomic modeling of irradiation-induced hardening

David Rodney

SIMAP-GPM2, INP Grenoble, CNRS/UJF, BP46, 38402 Saint Martin d'Hères, France

Available online 8 February 2008

Abstract

We review recent results obtained by Molecular Dynamics (MD) simulations on the elementary interaction mechanisms between dislocations and irradiation defects, with the aim to obtain a fundamental understanding of plasticity in irradiated metals. The reactions obtained included defect shear, drag and absorption in edge and screw dislocations. We present the state of the art in both FCC and BCC metals and discuss the challenges faced by MD simulations, in particular in BCC metals in order to realistically simulate the thermally-activated glide of screw dislocations in the presence of obstacles. ***To cite this article: D. Rodney, C. R. Physique 9 (2008).***

Résumé

Simulation atomique du renforcement de résistance aux radiations. Nous passons en revue des résultats récents obtenus par simulations en Dynamique Moléculaire (DM) sur les mécanismes élémentaires d'interaction entre dislocations et défauts d'irradiation, dans le but d'acquérir une connaissance approfondie de la plasticité des matériaux irradiés. Les réactions observées incluent le cisaillement, l'entraînement ainsi que l'absorption des défauts d'irradiation par des dislocations soient vis soient coin. Nous présentons l'état de l'art pour les métaux de structure Cubique à Faces Centrées (CFC) ainsi que Cubique Centrée (CC). Nous discutons les difficultés rencontrées dans les simulations par DM, en particulier dans les métaux CC, afin de simuler de façon réaliste le glissement thermiquement activé des dislocations en présence d'obstacles. ***Pour citer cet article : D. Rodney, C. R. Physique 9 (2008).***

PACS: 61.72.Bb

Keywords: Molecular dynamics; Irradiation; Plasticity

Mots-clés : Dynamique moléculaire ; Irradiation ; Plasticité

1. Introduction

Irradiation of crystals by high-energy particles, in particular neutrons, produces nano-scale defects that strongly affect the mechanical properties of irradiated crystals. The main feature, observed in all crystallographic structures and in mono- as well as polycrystals, is an increase of the elastic limit, followed, at high irradiation dose, by softening, i.e. a decrease of the flow stress with deformation [1]. This instability is due to a localization of the plastic deformation in shear bands that are clear, after deformation, of all irradiation defects visible in Transmission Electron Microscopy

E-mail address: david.rodney@inpg.fr.

1631-0705/$ – see front matter
doi:10.1016/j.crhy.2007.08.005

(TEM) and were thus called *clear bands* [2,3]. The nature of the irradiation defects depends on the material, the irradiation energy spectrum and the dose. In fission conditions, the defects consist mainly in clusters of either vacancies or interstitials. In Face-Centered Cubic (FCC) austenitic steels used in fission reactors, the defects visible in TEM are mostly faulted dislocation loops in the form of interstitial Frank loops (FL) [4,5], while in FCC copper, often used as a model FCC metal, the defects are clusters of vacancies, in the form of Stacking Fault Tetrahedra (SFT) [6]. In BCC ferritic steels, the defects consist of interstitial-type $\langle 100\rangle$- and $1/2\langle 111\rangle$-perfect loops [7,8]. In fusion conditions, in addition to the defect clusters mentioned above, a significant fraction of the neutrons have an energy above the (n,α)-reaction threshold and create He atoms [9]. The latter may remain in solution or gather to form He-bubbles that strongly interact with the dislocations responsible for the plastic deformation [10]. In all materials, the typical defect size is below 10 nm with a density $\sim 10^{24}$ m^{-3}, leading to average distances between defects in dislocation glide planes of the order of 50 nm.

To understand how irradiation defects influence the mechanical properties, one must know how they interact with the dislocations. In-situ TEM has been used to study the individual interactions between dislocations and SFTs [11] and FLs [12]. However, this technique is limited to large defects ($\sim$50 nm) and the resolutions, both spatial and temporal, are not sufficient to give access to the details of the interaction mechanism. On the other hand, the nanometric size of the defects is well adapted to atomic-scale simulations, and in particular to Molecular Dynamics (MD) and Statics (MS) simulations. Because of their large densities, the irradiation defects can be simulated with realistic sizes and densities in simulation cells containing only a few million atoms, which can be performed now-a-days on scalar computers when the interatomic interactions are modeled with semi-empirical potentials. The potentials most often used are based on the Embedded Atom Method (EAM) [13].

In the present article, we review MD simulations recently performed in FCC (Section 2) and BCC (Section 3) metals to better understand how dislocations and irradiation defects interact. The aim of these studies is two-fold. First, we want to understand the interaction mechanism and how irradiation defects are removed from the clear bands. Second, we want to compute directly from the simulations the resistance offered by the irradiation defects to the passage of the dislocations. This quantity is directly related to the elastic limit prior to plastic localization. As will be discussed in the article by Marc Fivel in the present issue [14], interaction mechanisms and defect resistance can be used in a multiscale approach as input parameters for larger-scale Dislocation Dynamics (DD) simulations to simulate at the micron-scale the dynamics of formation of clear bands.

2. State of the art in FCC crystals

The main FCC irradiation defects, i.e. interstitial FLs [15,16] and SFTs [17–21], as well as smaller glissile interstitial loops [22,23] were simulated in interaction with both edge and screw dislocations. In all cases, similar methodologies were employed. They are described in Section 2.1. The simulations led to a classification of the interaction mechanisms that is presented in Section 2.2. The relevance of these reactions with respect to possible scenarii of clear band formation is discussed in Section 2.3.

2.1. Computational model

The MD and MS techniques are classical; only the boundary conditions and the interatomic potentials are specific to the present studies. Fig. 1 presents the simulation cell in the case of a FCC crystal, but the same methodology applies to other crystallographic structures, such as BCC (see Section 3). Horizontal planes are {111} glide planes. The Y direction is along the dislocation Burgers vector (noted b hereafter). Edge (ED) and screw (SD) dislocations may be introduced by displacing all atoms according to their elastic displacement fields and the system is relaxed by MS to account for the boundary conditions. The latter are periodic both parallely and perpendicularly to the dislocation, in directions X and Y. A rigid shift of $b/2$ parallel to the Burgers vector is added in the X (respec. Y) surfaces for screw (respec. edge) dislocations in order to account for the plastic deformation imposed by the dislocation to the simulation cell (for details, see Ref. [15]). In the Z direction, fully free-, modified free- or rigid-boundary conditions are used depending on the loading condition.

In order to set the dislocation in motion, a shear stress σ_{YZ} may be created in the simulation cell in two ways which correspond to two loading conditions. The first condition is *stress controlled*, whereby extra forces in direction Y are added to the atoms in the upper and lower Z surfaces. The forces are in opposite directions in the two surfaces and are

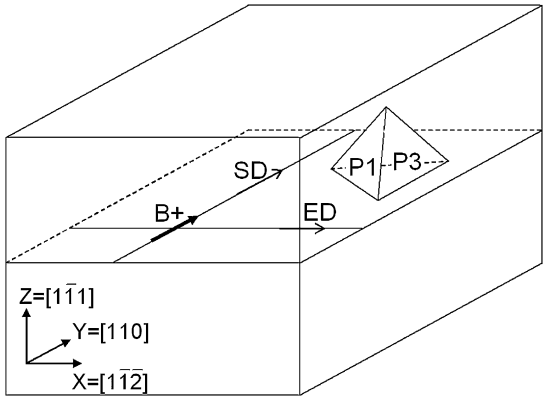

Fig. 1. Schematic representation of a simulation cell in a FCC crystal.

Fig. 1. Représentation schématique d'une boîte de simulation dans un cristal CFC.

such that the force per unit area in both surfaces is equal to σ_{YZ} [22]. The second loading condition is *strain controlled*, obtained by rigidly displacing the atoms in the upper and lower surfaces in direction Y in opposite directions in the two surfaces in order to impose a γ_{YZ} shear strain. The elastic part of this strain produces a stress: $\sigma_{YZ} = \mu\gamma^e_{YZ}$ [24]. In the case of FCC crystals, both methods yield similar results in the calculation of obstacle resistances, in contrast with BCC crystals where screw dislocations are very sensitive to the boundary conditions, for reasons discussed in Section 3. A new method, allowing for strain-controlled loading without rigid boundary conditions was recently proposed [25], but will not be used here. If the strain (respect. stress) is increased at each time step, the simulation is performed at constant strain- (respect. stress-) rate. Since the simulation time is limited to a few nanoseconds, the strain-rates thus obtained are very large compared to typical tensile tests, 10^7 s^{-1} compared to 10^{-4} s^{-1}. The consequence, further discussed in Section 3, is that thermally-activated processes with activation energies above 0.5 eV are difficult to study by direct MD simulations.

Interatomic interactions are modeled using semi-empirical many-body potentials, most often of the EAM type [13]. With such potentials, the elastic constants, lattice parameter, vacancy formation energy and some surface energies are well reproduced. However, for the purpose of dislocation modeling in FCC metals, the main property is the Stacking Fault Energy (SFE) that controls the dissociation distance of perfect $1/2\langle 110\rangle\{111\}$ dislocations. This property is discriminant because the SFE, if not explicitly introduced in the fitting procedure, is systematically very low. EAM potentials with reasonable SFEs have been developed for pure metals: Nickel [26,27], Cu [28], Al [29]. On the other hand, austenitic stainless steels are complex alloys whose chemistry cannot be reproduced with EAM potentials. Up to now, the effect of alloying elements has been studied only in model solid-solutions [30–34]. With respect to dislocations, the main characteristic of austenitic alloys is to have a SFE that is lower than all pure FCC metals and that depends on the temperature [35]. In the following, we limit ourselves to pure metals, and in particular employ the copper EAM potential developed by Mishin et al. [28] that predicts a SFE representative of austenitic steels at 600 K [16]. Realistic EAM potentials are more difficult to construct for BCC metals, in particular α-Iron, as will be discussed in Section 3.

2.2. Interaction mechanisms

We systematically studied how edge and screw dislocations interact with either FLs [16] or SFTs [20]. To achieve this, we placed an irradiation defect in front of a dislocation and performed either a stress- or a strain-controlled MD simulation. The interaction mechanisms depend on several factors including the relative configuration between the defect and the dislocation, the temperature, the stress- or strain-rate. The reactions are presented in the following using a classification proposed in the case of SFTs [20] but which applies equally well to FLs, showing that both types of defects interact similarly with dislocations.

The first type of reaction is called $R1/R2$. It corresponds to a simple *shear* of the irradiation defect by the passage of the dislocation and concerns both edge and screw dislocations at low temperature and/or high strain rates. It is illustrated in Fig. 2 in the case of a screw dislocation in interaction with a SFT. The dislocation glides through the SFT

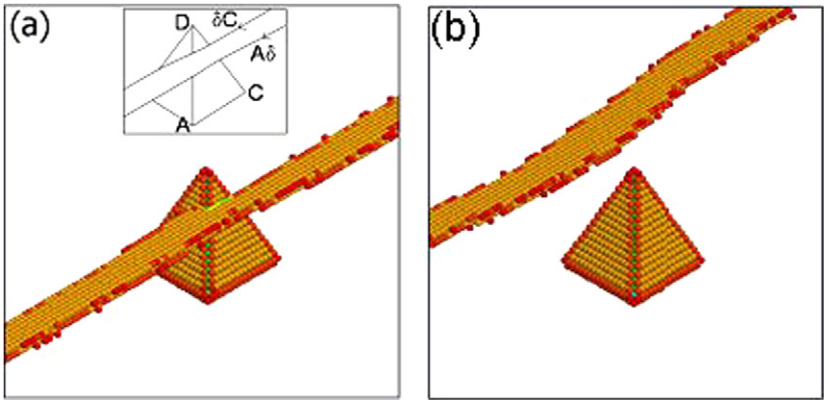

Fig. 2. Shearing ($R1$) of a SFT by a screw dislocation (from Ref. [20]).
Fig. 2. Cisaillement ($R1$) d'un tétraèdre de fautes d'empilement par une dislocation vis.

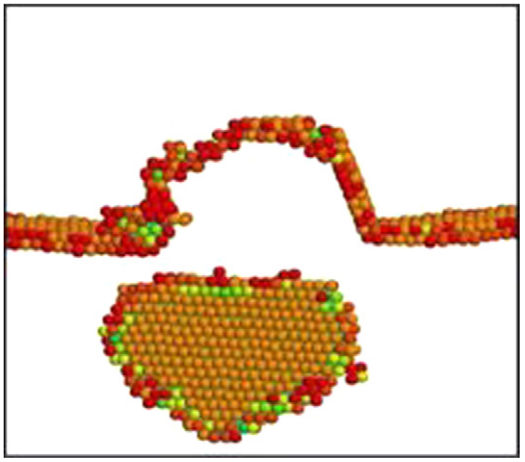

Fig. 3. Partial absorption ($R3$) of a FL by an edge dislocation (from Ref. [16]).
Fig. 3. Absorption partielle ($R3$) d'une boucle de Frank par une dislocation coin.

that retains its initial structure and is only sheared by the dislocation Burgers vector, thus acquiring a step. Two cases are then possible. As shown in Fig. 2(b), the step may be mobile on the defect and eliminate (case $R1$), leading to a full reconstruction of the defect after the passage of the dislocation. The second case ($R2$) is when the step is stable. Damage may then be accumulated on the defect by multiple dislocation passages, leading to a progressive shear of the defect. In analogy with alloys with shearable precipitates [3], if enough dislocations shear the defect, the latter may decrease in size until it becomes unstable and may be absorbed on the dislocation line and be dragged away. This type of reaction was observed with small glissile loops [22,23]. In both cases, the damage is limited and $R1/R2$ reactions thus play a limited role in the formation of clear bands.

The second type of reaction, called $R3$, concerns edge dislocations that can partially *absorb* irradiation defects along their line. This reaction is illustrated in Fig. 3 for the case of an edge dislocation that absorbed the upper part of a FL. As can be seen, the edge dislocation locally climbed and acquired superjogs. This type of reaction requires thermally activated processes and is observed at high temperature and/or low strain-rates. The superjogs on the edge dislocation are mobile in the dislocation glide direction and can be dragged away. This *drag* effect is efficient to remove defects from a clear band. However, in the FL case, the reaction occurs only in one specific configuration at high temperature (600 K), while in all other configurations and at lower temperatures (300 K), edge dislocations shear the irradiation defects according to $R1/R2$ reactions.

The third type of reaction, called $R4$, concerns screw dislocations that can *absorb* an irradiation defect along their line. In the FL case, the absorption is complete while with SFTs, we observed only partial absorptions, according to an

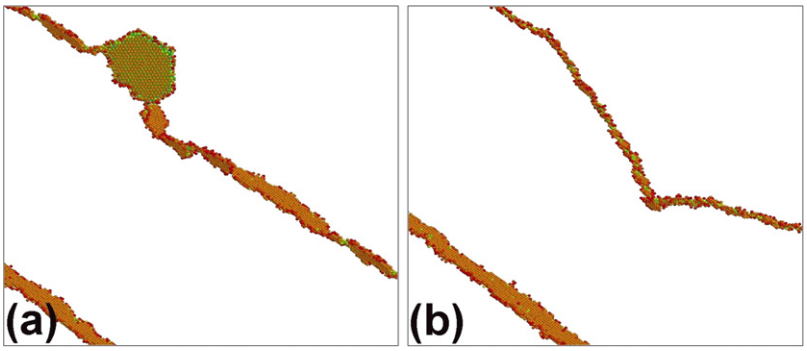

Fig. 4. Complete absorption ($R4$) of a FL by a screw dislocation (from Ref. [16]).
Fig. 4. Absorption complète ($R4$) d'une boucle de Frank par une dislocation vis.

incomplete Kimura–Maddin mechanism [36]. The absorption reaction, illustrated in Fig. 4, implies cross-slip events of the screw dislocation, that are promoted by the short-range interaction between the dislocation and the defect, but remain, nevertheless, thermally activated. This reaction is thus observed at high temperature and/or low strain rate. The defect, once absorbed, forms a helical turn on the screw dislocation as shown in Fig. 4(b). This structure is a strong obstacle to the glide of the dislocation because the helical turn is mobile only in the Burgers vector direction, i.e. along the dislocation and not in the glide direction. Helical turns are in fact stronger obstacles than the initial defects because they do not remain localized but expand along the entire length of the dislocation. In the FL case, the reaction occurs in all configurations. For the clear band to further develop, the screw dislocation must unpin from the helical turn. This unpinning involves the activation in a new glide plane of a segment of the helical turn, that bows out and forces the helical turn to close onto itself, thus allowing for unpinning via an Orowan process.

2.3. Discussion: edge versus screw

From the above description of the interaction mechanisms, we conclude that edge and screw dislocations behave very differently in the presence of irradiation defects. Edge dislocations mainly shear the defects but remain mobile when acquiring superjogs, while screw dislocations mostly absorb the loops and become strongly pinned by the formation of helical turns. Screw dislocations are thus the main engine for the formation of clear bands. Edge dislocations are important for defect removal since when screw dislocations are activated, they may push the helical turns towards edge portions where they become glissile superjogs that are dragged away towards the band edges. If two activated segments meet, they may undergo an Orowan process around a cluster of superjogs, creating heavily jogged prismatic loops, as observed in TEM by Sharp [2]. In this process, the initial large density of small irradiation defects is transformed in a smaller density of larger loops that offer a smaller resistance, thus leading to plastic instability. Helical turns also play a role in clear band broadening since the simulations showed that when a screw dislocation unpins from a helical turn, it is not re-emitted in its initial glide plane and can thus interact with defects in a new glide plane. These predictions based on MD simulations are currently tested in larger scale DD simulations (see the article by M. Fivel in the present issue [14]).

3. Challenges in BCC crystals

Plasticity in BCC crystals is very different from FCC crystals. It is characterized by an elastic limit that strongly depends on the temperature up to typically room temperature, is asymmetrical in tension and compression and is influenced by compressive stresses [37]. The origin of these features can be traced down to the atomic-scale and the non-planar core structure of the screw dislocations [38], which implies a high lattice-friction Peierls stress strongly influenced by non-glide stresses [39]. Comparatively, edge dislocations have a much higher mobility, resulting in dislocation microstructures made of long screw segments separated by short edge kinks. The elastic limit of BCC crystals is thus mainly controlled by the mobility of the screw dislocations. The study of the latter at the atomic scale is difficult, for at least three reasons: (1) the non-planar core structure of screw dislocations is difficult to reproduce

with semi-empirical interatomic potentials, (2) the Peierls stress is strongly influenced by the boundary conditions applied to the simulation cell and (3) the motion of screw dislocations is thermally activated below the Peierls stress and can be slow compared to the time-scales attainable by MD simulations. Points (1) and (3) are detailed below. For point (2), see Ref. [40].

3.1. Realism of interatomic potentials

BCC dislocations have a $1/2\langle 111\rangle$ Burgers vector. The core structure of screw dislocations is best illustrated using Differential Displacement Maps [38], as shown in Fig. 5 which presents BCC crystals in projection along a $\langle 111\rangle$ direction. Atoms visible in this figure correspond to atomic columns. A screw dislocation was inserted in the crystals with a line parallel to the $\langle 111\rangle$ direction of projection. The arrows joining first-neighbor columns have a length proportional to the difference in displacement between the two columns and are scaled such that an arrow of length equal to the inter-column distance corresponds to a difference of displacement of $b/3$. As shown in Fig. 5, the $\langle 111\rangle$ direction contains 3 families of {110} planes. Figs. 5 (a) and (b) were obtained with two different EAM potentials that both reproduce α-Iron (for (a), Ref. [41] and for (b), Ref. [42]). In Fig. 5(b), the core structure is asymmetrical in the {110} planes, with a long arrow on one side of the core without counterpart on the other side. This type of structure is predicted by most interatomic potentials. It is said to be three-fold or *degenerate* because it comes in two variants: the one shown here and the other obtained by changing the side of the arrows on all 3 {110} planes with respect to the dislocation core. Defining the core structure with precision is of prime importance because a dislocation with such a core structure moves under stress by a *zig-zag* motion, whereby the dislocation changes variant after each displacement from one Peierls valley to the next [43]. The two variants move on different {110} planes, resulting in an average {112} glide plane, while experimentally, it has been known since the 1970s that glide in α-Iron occurs on {110} planes at low temperatures and at all temperatures when a {110} plane is of maximum resolved shear stress [44,45]. This contradiction between atomic-scale simulations and experiments was recently explained by ab initio calculations that showed that the dislocation core is in fact symmetrical, as shown in Fig. 5(a) [46,47]. This figure was obtained with the only EAM potential published to-date, developed by Mendelev et al. [41], that predicts a symmetrical, also said to be six-fold or *non-degenerate* structure. Since the core remains unchanged after each elementary displacement from one Peierls valley to the next, the dislocation can glide on a {110} plane, in agreement with the experiments.

Another difficulty concerns the Peierls stress which is usually predicted to be 2 to 3 times higher than the values extrapolated from experiments [49–52,46]. This discrepancy may, however, be due to a confusion between the critical stress above which the motion of a rigid straight dislocation becomes athermal, considered in static simulations, and the critical stress above which the activation enthalpy for kink-pair nucleation becomes zero, which is the relevant Peierls stress in dynamical simulations and experiments. It has recently been shown [25] that the latter may be significantly smaller than the former.

Up-to-now, α-Iron has been used to model the ferritic/martensitic steels studied in fission and fusion programs. However, all studies were performed with potentials that predict a degenerate core structure, mostly the potential developed by Ackland et al. [53], and thus with a screw dislocation glide plane in contradiction with experiments. Also, the only available binary potential for the Fe–He system, required to study the influence of He on the elastic limit, is based on the same Ackland potential [54,55]. Authors were thus compelled to study either edge dislocations which

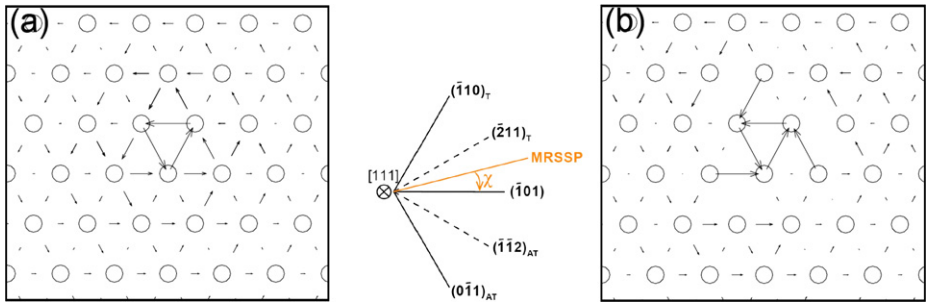

Fig. 5. Differential displacement maps of non-degenerate (a) and degenerate (b) screw dislocation cores in α-Iron (from Ref. [40]).

Fig. 5. Cartes de déplacements différentiels de cœurs non-dégénéré (a) et dégénéré (b) de dislocations vis dans un crystal de Fer-α.

can be geometrically forced to glide on a {110} plane [56–59], or screw dislocations, knowing that the information obtained is only a first approximation [60,61].

There is thus a strong need for developing more realistic interatomic potentials. Mendelev potential has its own limitations. For example, in the context of plasticity, a {110} glide plane is obtained but is unstable [40]: increasing the temperature induces a rotation of the glide plane towards a {112} plane. Also, dislocation jumps occur by half kinks, in contradiction with recent ab-initio calculations [62].

3.2. Time-scale limitation

The Peierls stress in α-Iron predicted by interatomic potentials is around 1 GPa. Below this value, the motion of the dislocation is thermally-activated. As illustrated in Fig. 6, the motion is composed of waiting periods during which the dislocation is immobile at the bottom of a Peierls valley (aligned in a $\langle 111 \rangle$ direction), separated by the thermally-activated nucleation of a kink-pair that locally brings the dislocation in the next Peierls valley. The subsequent expansion of the kink-pair progressively transfers the rest of the dislocation in the next Peierls valley [63].

The average waiting time follows a thermally-activated law, proportional to $\exp(H(\sigma)/kT)$, where $H(\sigma)$ is the kink-pair activation enthalpy and kT the thermal energy. Since the time scale accessible to MD simulations is of the order of a few nanoseconds, the average waiting time must be small compared to this value, thus imposing a low value of the activation ratio H/kT. As orders of magnitude, in MD simulations, $H/kT \sim 10$ [48,25], while experimentally $H/kT \sim 30$ [64]. These values reflect the fact that the waiting time is less than a nanosecond in MD simulations, while it is in the microsecond range experimentally. Since the activation enthalpy decreases with the stress, MD simulations are limited to a range of relatively high temperatures and/or stresses, higher than in experiments. With a thermal energy of 0.05 eV at 600 K, thermally-activated processes with activation energies greater than about 0.5 eV cannot be captured with direct MD simulations.

This limitation is the main constraint on MD simulations. It has consequences in both FCC and BCC crystals. In FCC crystals, complex reactions, such as the $R3$ and $R4$ absorptions presented in Section 2.2, require thermally-activated processes, and in particular cross-slip events. The probability of such events increases with the time the dislocation spends in contact with the defect. The latter being much shorter than experimental values, MD simulations favor less complex reactions, such as $R1/R2$ shear reactions. The case of BCC crystals is more difficult because the

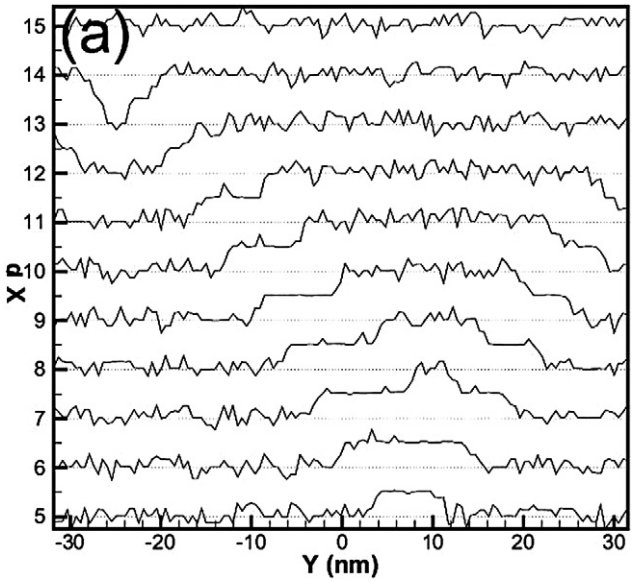

Fig. 6. Nucleation and propagation of two half kink-pairs on a screw dislocation. The lines follow the center of gravity of the core atoms along the dislocation. For the sake of clarity, the curves are shifted with respect to each other by one Peierls valley (from Ref. [40]).

Fig. 6. Nucléation et propagation de deux demi double-crans sur une dislocation vis. Les lignes suivent le centre de gravité des atomes de coeur le long de la dislocation. Par souci de clareté, les courbes ont été décalées d'une vallée de Peierls les unes par rapport aux autres.

background stress applied to simply move the dislocation through the Peierls valleys in a timescale compatible with the MD simulations amounts to several hundred MPa. Consequently, only strong obstacles with resistances above this background stress can be studied since the dislocation will glide through the weaker obstacles without really interacting with them. A discussion on thermally-activated obstacle by-passing can also be found in Ref. [65].

3.3. Applications

Keeping in mind the limitations discussed above, several studies have been performed on the interaction of edge and screw dislocations in α-Iron with irradiation defects in the form of interstitial prismatic loops [60,56,57], He atoms either isolated [61,58] or in bubbles [59] as well as voids and precipitates [66].

Concerning the interaction between substitutional and interstitial He atoms with dislocations [61,58], it was shown that the He atoms strongly bind to the tension side of edge dislocations, while they bind to screw dislocations only if they are directly in the dislocation core. In both cases however, the activation energy for migration along the dislocation line is small, leading to pipe diffusion. The resistance of He-bubbles strongly depends on their He-content. The resistance may be strong for large He-contents, in which case a large confinement pressure builds up that promotes loop punching [59].

For the interaction between prismatic loops and edge dislocations [56,57], it was shown that small loops may undergo Burgers vector flips to align with that of the dislocation and are then dragged away. Similar results were found in FCC crystals [22,23]. Larger loops cannot change Burgers vector spontaneously. They form sessile junctions with the edge dislocation and offer a strong resistance. Subsequent glide of the junction segment leads to a transformation of the attached loop into a pair of superjogs on the edge dislocation.

4. Conclusions

We have shown that the atomic-scale study of plasticity in FCC metals is well advanced, at least in pure metals, with systematic studies of edge and screw dislocations in interaction with the irradiation defects mainly observed in TEM. In comparison, studies in BCC crystals are much less advanced, the reasons being two-fold: the realism of interatomic potentials for this structure and the difficulty to account for the thermally-activated motion of screw dislocations with MD simulations. The same limitations apply to HCP metals such as Zirconium [67].

Future studies will require more reliable interatomic potentials. Potentials for binary systems are also much needed, and, in particular, an accurate potential for the Fe–C system to better account for the thermodynamics of steels. As for the time-scale, the progress in computing power will certainly not allow to bridge the gap between the strain-rates in MD simulations (10^7 s^{-1}) and in experiments (10^{-4} s^{-1}). On the other hand, progress can be made through the use of static methods, such that the Nudged Elastic Band method [68], that allows for the calculation of activation energies and enthalpies on complex transition paths.

Acknowledgements

The work on FLs in FCC metals presented in Section 2 was part of the PhD work of Thomas Nogaret. It was funded by the European PERFECT project (No. FI60-CT-2003- 508840). The results on SFTs were obtained in collaboration with Dr. Yuri Osetsky and Prof. D. Bacon. The work on BCC metals presented in Section 3 was part of the PhD work of Julien Chaussidon. The author thanks Dr. F. Willaime and L. Ventelon for numerous and stimulating discussions.

References

[1] M. Victoria, N. Baluc, C. Bailat, Y. Dai, M. Luppo, R. Schaüblin, B.N. Singh, J. Nucl. Mater. 276 (2000) 114.
[2] J.V. Sharp, Philos. Mag. 16 (1967) 77–96.
[3] A. Luft, Progr. Mater. Sci. 35 (1991) 97.
[4] P. Maziasz, J. Nucl. Mater. 205 (1993) 118.
[5] C. Pokor, Y. Bréchet, P. Dubuisson, J.P. Massoud, A. Barbu, J. Nucl. Mater. 326 (2004) 19.
[6] B.N. Singh, S.J. Zinkle, J. Nucl. Mater. 206 (1993) 212.
[7] B. Masters, Philos. Mag. 11 (1965) 881.
[8] B. Eyre, R. Bullough, Philos. Mag. 12 (1965) 31.

[9] E. Bloom, S. Zinkle, F. Wiffen, J. Nucl. Mater. 329–333 (2004) 12.
[10] D. Gelles, G. Hankin, M. Hamilton, J. Nucl. Mater. 251 (1997) 188.
[11] Y. Matsukawa, S.J. Zinkle, J. Nucl. Mater. 329–333 (2004) 919.
[12] M. Suzuki, A. Sato, T. Mori, N. Nagakawa, H. Shiraishi, Philos. Mag. A 65 (1992) 1309.
[13] M. Daw, M. Baskes, Phys. Rev. B 29 (1984) 6440.
[14] M.C. Fivel, C. R. Physique 9 (3–4) (2008) 427.
[15] D. Rodney, Acta Mater. 52 (2004) 607.
[16] T. Nogaret, C. Robertson, D. Rodney, Philos. Mag. 87 (2007) 945.
[17] B.D. Wirth, V.V. Bulatov, T. de la Rubia, J. Eng. Mater. Technol. 124 (2002) 329.
[18] Y.N. Osetsky, R.E. Stoller, D. Rodney, D.J. Bacon, Mater. Sci. Eng. A 400–401 (2005) 370.
[19] P. Szelestey, M. Patriarca, K. Kaski, Model. Simul. Mater. Sci. Eng. 13 (2005) 541.
[20] Y.N. Osetsky, D. Rodney, D.J. Bacon, Philos. Mag. 86 (2006) 2295.
[21] J.S. Robach, I.M. Robertson, H.J. Lee, B.D. Wirth, Acta Mater. 54 (2006) 1679.
[22] D. Rodney, R. Phillips, Phys. Rev. Lett. 82 (1999) 1704.
[23] D. Rodney, G. Martin, Phys. Rev. B 61 (2000) 8714.
[24] Y. Osetsky, D. Bacon, Model. Simul. Mater. Sci. Eng. 11 (2003) 427.
[25] D. Rodney, Phys. Rev. B (2007), in press.
[26] J. Angelo, N. Moody, M. Baskes, Model. Simul. Mater. Sci. Eng. 3 (1995) 289.
[27] Y. Mishin, D. Farkas, D. Papaconstantopoulos, Phys. Rev. B 59 (1999) 3393.
[28] Y. Mishin, D. Farkas, M. Mehl, D. Papaconstantopoulos, A. Voter, J. Kreuss, Phys. Rev. B 63 (2001) 224106.
[29] F. Ercolessi, J. Adams, Europhys. Lett. 26 (1994) 583.
[30] E. Rodary, D. Rodney, L. Proville, Y. Bréchet, G. Martin, Phys. Rev. B 70 (2004) 054111.
[31] L. Proville, D. Rodney, Y. Bréchet, G. Martin, Philos. Mag. 86 (2006) 3893.
[32] J. Marian, A. Caro, Phys. Rev. B 74 (2006) 024113.
[33] D. Olmsted, L. Hector, W. Curtin, J. Mech. Phys. Sol. 54 (2006) 1763.
[34] K. Tapasa, D. Bacon, Y. Osetsky, Model. Simul. Mater. Sci. Eng. 14 (2006) 1153.
[35] R.M. Latanision, A.W. Ruff, Metall. Trans. 2 (1971) 505.
[36] H. Kimura, R. Maddin, Academic Press, New York, 1965, p. 319.
[37] J. Christian, J. Metall. Trans. A 14 (1983) 1237.
[38] V. Vitek, Cryst. Lattice Defects 5 (1974) 1.
[39] M. Duesbery, V. Vitek, Acta Mater. 46 (1998) 1481.
[40] J. Chaussidon, M. Fivel, D. Rodney, Acta Mater. 54 (2006) 3407.
[41] M. Mendelev, S. Han, D. Srolovitz, G. Ackland, D. Sun, M. Asta, Philos. Mag. 83 (2003) 3977.
[42] G. Simonelli, R. Pasianot, E. Savino, Mater. Res. Soc. Symp. Proc. 291 (1993) 567.
[43] M. Wen, A. Ngan, Acta Mater. 48 (2000) 4255.
[44] W. Spitzig, A. Keh, Acta Metall. 18 (1970) 611.
[45] W. Spitzig, A. Keh, Acta Metall. 18 (1970) 1021.
[46] C. Woodward, S.I. Rao, Phys. Rev. Lett. 88 (2002) 216402.
[47] S. Frederiksen, K. Jacobsen, Philos. Mag. 83 (2003) 365.
[48] C. Domain, G. Monnet, Phys. Rev. Lett. 95 (2005) 215506.
[49] Z. Basinski, M. Duesbery, G. Murthy, Acta Metall. 29 (1981) 801.
[50] M. Duesbery, Z. Basinski, Acta Metall. Mater. 41 (1993) 643.
[51] K. Ito, V. Vitek, Philos. Mag. A 81 (2001) 1387.
[52] L. Yang, P. Söderlind, J. Moriarty, Philos. Mag. A 81 (2001) 1355.
[53] G. Ackland, D. Bacon, A. Calder, T. Harry, Philos. Mag. A 75 (1997) 713.
[54] K. Morishita, R. Sugano, B. Wirth, J. Nucl. Mater. 323 (2003) 243.
[55] L. Ventelon, B. Wirth, C. Domain, J. Nucl. Mater. 351 (2006) 119.
[56] Z. Rong, Y. Osetsky, D. Bacon, Philos. Mag. 85 (2005) 1473.
[57] D. Bacon, Y. Osetsky, Z. Rong, Philos. Mag. 86 (2006) 3921.
[58] H. Heinisch, F. Gao, R. Kurtz, E. Le, J. Nucl. Mater. 351 (2006) 141.
[59] R. Schäublin, Y.L. Chiu, J. Nucl. Mater. 362 (2007) 152.
[60] J. Marian, B. Wirth, R. Schaeublin, G. Odette, J. Perlado, J. Nucl. Mater. 323 (2003) 181.
[61] H. Heinisch, F. Gao, R. Kurtz, J. Nucl. Mater. 367–370 (2007) 311.
[62] L. Ventelon, F. Willaime, in preparation.
[63] A. Seeger, Philos. Mag. 1 (1956) 651.
[64] D. Brunner, J. Diehl, Phys. Stat. Sol. (a) 124 (1991) 455.
[65] K. Tapasa, D.J. Bacon, Yu.N. Osetsky, Acta Mater. 55 (2007) 93.
[66] Y.N. Osetsky, D.J. Bacon, V. Mohles, Philos. Mag. 83 (2003) 3623.
[67] R.E. Voskoboinikov, Y.N. Osetsky, D.J. Bacon, Mater. Sci. Eng. A 400–401 (2005) 49 and 54.
[68] G. Mills, H. Jonsson, Phys. Rev. Lett. 72 (1994) 1124.